Available online at www.sciencedirect.com
ScienceDirect
Applied Surface Science 253 (2007) 6301–6304
applied surface science
www.elsevier.com/locate/apsusc

Coherent phonon excitation in bismuth

Alexander Q. Wu, Xianfan Xu *

School of Mechanical Engineering, Purdue University, West Lafayette, IN 47907, USA

Available online 26 January 2007

Abstract

Ultrafast time-resolved reflectivity of a bismuth thin film evaporated on a silicon substrate is measured to investigate coherent phonons in bismuth. The reflectivity result is analyzed by a linear chirp approximation to obtain the time dependent frequencies of coherent phonons. Not only the optical modes are detected, which are generated by a combination of impulsive stimulated Raman scattering and displacive excitation of coherent phonon, acoustic phonon modes are also observed, which are emitted by the A_{1g} optical phonon.

PACS : 63.20.Kr

Keywords: Femtosecond laser; Bismuth; Coherent phonon; Raman scattering; Displacive excitation

Time-resolved reflectivity and transmissivity measurements are valuable tools to study phonon dynamics in samples irradiated by ultrafast laser pulses. For example, coherent optical phonons in semimetals such as bismuth (Bi) and antimony (Sb) were studied by Cheng et al. through time-resolved reflectivity measurements [1,2]. Their generation was attributed to the mechanism called displacive excitation of coherent phonon (DECP) [3], which predicated that only the totally symmetric A_{1g} mode can be excited. The ions are induced to vibrate coherently by an external pump laser as the lattice equilibrium with electronically excited states is different from that of the ground states. Such vibrations in Bi have been directly observed by time-resolved X-ray measurements [4]. Later, it was suggested that DECP is a special case of impulsive stimulated Raman scattering (ISRS) [5]. More recently, Stevens et al. found that the stimulated Raman scattering could be described by two separate tensors, one is the standard Raman susceptibility and the other accounts for the electrostrictive force acting on the ions [6]. The generation of coherent phonons in transparent materials can be described by ISRS as these two tensors have the same real components. On the other hand, there could be a DECP mechanism if the imaginary term dominates in the tensor for the electrostrictive force. This occurs in opaque materials such as Bi, where a combination of ISRS and DECP is possible to generate coherent phonons [6]. Contrary to the regular laser absorption where the laser energy is initially absorbed by electrons and then coupled to lattice [7], coherent phonon generation is a direct energy absorption process, which can result in a nonthermal melting without heating the lattice to the melting temperature [8].

In this paper, we report observations of both optical and acoustic coherent phonons in Bi pumped by femtosecond pulses. A commercial Ti:sapphire ultrafast regenerative amplified laser is used in our experiments. It operates at a center wavelength of 800 nm, maximum energy of 1 mJ per pulse, and a repetition rate of 1 kHz. The measurement of single shot autocorrelation shows the pulsewidth is 80 fs full width at half maximum (FWHM). The horizontally polarized output beam is split into two beams, pump beam (80%) and probe beam (20%). The pump beam is passed through a mechanical delay line consisting of a hollow cube retro-reflector mounted on a linear travel stage. The horizontally polarized pump beam is focused normally on the sample by a lens with a focal length $f = 300$ mm. The vertically polarized probe beam is obliquely focused with an incident angle of about 14° by a lens with a focal length $f = 100$ mm. The reflected probe beam is collected by another 100 mm lens and is measured by a balanced detector (Newfocus 2307). A reference beam split from the probe beam is also input into the balanced detector to improve the signal-to-noise ratio. Appropriate neutral density filters (ND) are used before the detector to ensure that the detector operates in the linear regime. Polarizers are also inserted before the balanced

* Corresponding author. Tel.: +1 765 494 5639; fax: +1 765 494 0539.
E-mail address: xxu@ecn.purdue.edu (X. Xu).

0169-4332/$ – see front matter © 2007 Elsevier B.V. All rights reserved.
doi:10.1016/j.apsusc.2007.01.043

detector to minimize the noise scatted from the pump beam. The laser energy is adjusted by using ND filters and half-wave-plate/polarizer combinations. The pump beam is chopped at around 100 Hz. The signal from the balanced detector is measured by a lock-in amplifier. The Bi thin film is thermally evaporated on a polished silicon substrate. The thickness is around 100 nm, which is six times thicker than the penetration depth of the laser beam at 800 nm (the linear absorption coefficient of Bi at 800 nm is $\sim 6 \times 10^5$ cm^{-1} [12]). The sample is mounted on a 3D computer controlled stage. A CCD imaging system with total magnification of 500× is used to ensure the probe beam is overlapped with the center of the pump beam at the sample surface. Scanning knife-edge measurements show the pump and probe beam radius at the sample surface is 530 and 100 μm, respectively.

Fig. 1 shows the time-resolved measurements of relative change of reflectivity $\Delta R/R$ with different laser fluences, which are much lower than the damaged threshold value ~22 mJ/cm^2. A weaker probe beam with a fixed fluence of 16 μJ/cm^2 is used to minimize its effect on the excited state generated by the pump beam. For high laser fluences, the data before time zero are shifted for clarity. The reflectivity increases instantaneously during the pump pulse duration, and then drops gradually with the increase of time delay. The damping oscillatory coherent phonon signal is superimposed on a slowly decaying background which is due to the change of electronic susceptibility by the photoexcited carriers [9,10]. In order to analyze the reflectivity in detail, we use the following equation to fit the experimental data:

$$\frac{\Delta R}{R} = U_{(t-t_0)}\{A_e\left[-\exp\left(-\frac{t-t_0}{\tau_R}\right)+\exp\left(-\frac{t-t_0}{\tau_F}\right)\right] + A_p \exp\left(-\frac{t-t_0}{\tau_P}\right)\cos[(2\pi\nu_0 + \beta(t-t_0))(t-t_0)+\varphi]\} \quad (1)$$

The background reflectivity is described by the first term [11], where A_e, τ_R, and τ_F are the amplitude, the buildup time, and the decay time of the photoexcited carriers, respectively. The second term accounts for coherent phonons [12], where A_p, τ_p, ν_0, β, and φ are the amplitude, the dephasing time, the coherent phonon frequency, the chirp coefficient, and the initial phase of coherent phonon, respectively. $U_{(t)}$ is the unit step function. t_0 is a constant describing the initial time of overlapping between the probe and the pump beams. An example of data fitting by Eq. (1) is shown in Fig. 1(b). It can be seen that Eq. (1) gives a good description for the reflectivity data for the entire time duration where the phonon oscillatory signal is obvious. It is noted that it is important to include the variation of the phonon frequency with time (the chirp term β) in the data analysis. The result of curve fitting does not agree well with the experimental data if the chirp term is not considered. As shown in the inset of Fig. 1(b), without including the chirp term, a large phase difference between the experimental data and the fitted results appears at later times.

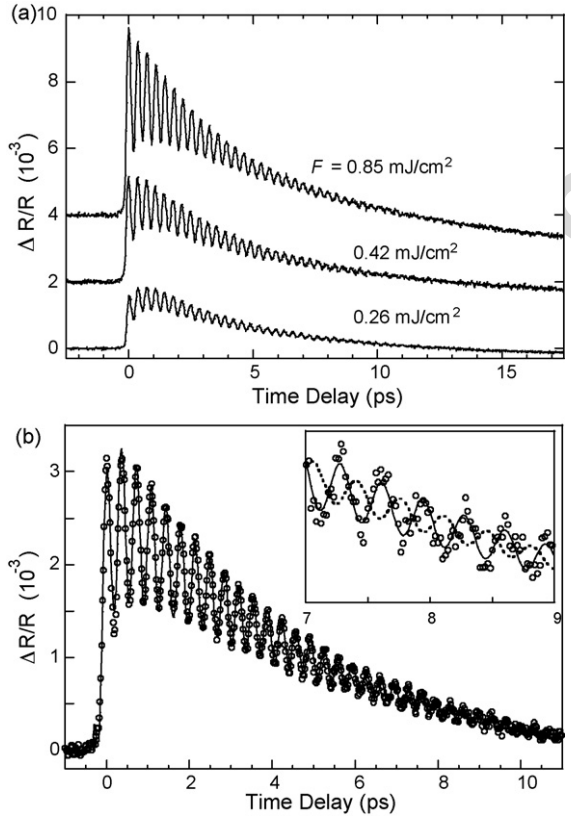

Fig. 1. (a) Time dependence of reflectivity change $\Delta R/R$ at three different pump fluences 0.26, 0.42, and 0.85 mJ/cm^2. The probe fluence is 16 μJ/cm^2. Negative value of time delay means the pump beam is behind the probe beam. Two curves are vertically translated for clarity in the plot. (b) Fitted curve based in Eq. (1) in case of $F = 0.42$ mJ/cm^2. Inset: the effect of fitting with/without chirp term in Eq. (1). Open circle: experimental data; solid: fitted curve with chirp term; dash: fitted curve without chirp term.

Parameters used in Eq. (1) for fitting the experimental data show some fundamental processes of phonon generation, dephasing, and phonon–phonon interaction. Fig. 2 shows the pump fluence dependence of (a) amplitude of A_e and A_p, (b) buildup time τ_R, decay time τ_F, and dephasing time τ_P, and (c) coherent phonon frequency ν_0 and chip coefficient β fitted by Eq. (1). With increasing of laser fluence, the buildup time τ_R is decreased as photoexcited carriers are generated more quickly, both amplitudes of A_e and A_p are increased linearly as more photoexcited carriers are excited. When the photoexcited carrier density is increased, the crystal lattice will be weakened, resulting in a softer phonon with a decreased phonon frequency [9,13]. At the same time, the diffusion of photoexcited carriers on the surface will be slower because of the reduced ambipolar diffusion coefficient [14], resulting in a slight increase in decay time τ_F [15]. While the elongated photoexcited carriers should be beneficial for coherent phonon existence, the decreased dephasing time τ_P clearly shows that other factors such as phonon–phonon interaction, which extinguishes coherent phonons, will become stronger in the case of higher laser fluence. This is also consistent with the value of chirped coefficient β, which shows how fast the soft (low frequency) phonons recover the normal frequency value.

Fig. 3 shows the Fourier transformed (FT) amplitude spectra from the experimental data in Fig. 1(a). The high values near zero are due to the non-oscillatory background signal. Distinct

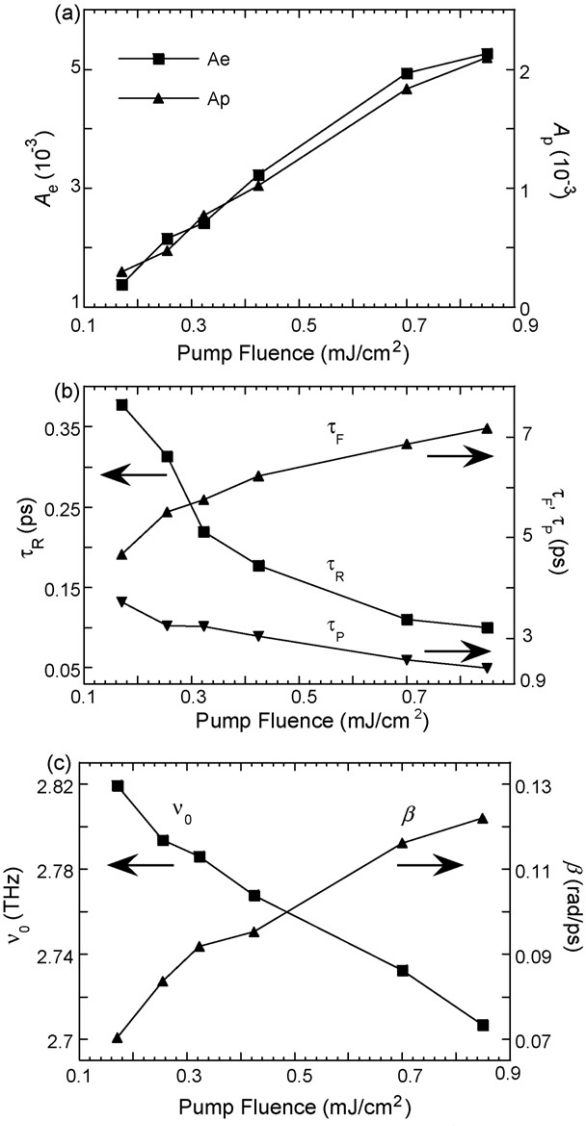

Fig. 2. Pump fluence dependence of (a) amplitude of A_e and A_p, (b) buildup time τ_R, decay time τ_F, and dephasing time τ_P, and (c) coherent phonon frequency ν_0 and chip coefficient β. Error bars are not included as the relative errors of the fitted coefficients are less than 1%.

peaks of optical phonons are obtained near 2.9 THz. (Note that due to the difference in mathematic formulation, the phonon frequencies obtained using FT and using Eq. (1) are slightly different.) As the laser fluence is increased, the phonon frequency is red-shifted and asymmetrically broadened to the lower frequency side. The asymmetrical broadening of the peaks is due to the initial red-shift of the soft phonon, causing the frequency broadening to the lower frequency side.

The interesting feature in Fig. 3 is that phonon oscillations at frequencies other than the A_{1g} optical phonon are observed at high laser fluence. Not only the E_g phonon at the frequency of 2.20 THz but also four other frequency peaks appear on the low frequency side of the phonon spectra. These peaks are almost equally spaced with $\Delta\nu = 0.39 \pm 0.05$ THz. (Note: the frequency resolution in Fig. 3 is 0.05 THz.) The appearance of the E_g phonon together with the A_{1g} phonon shows the coherent

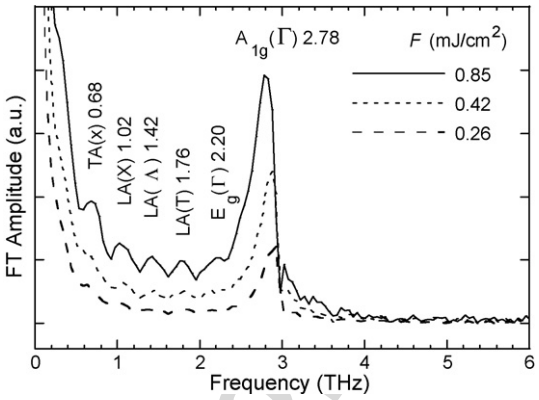

Fig. 3. Fourier transformed spectra corresponding to Fig. 1(a). Peaks of phonon are also labeled.

phonon generation in Bi is a combination of ISRS and DECP as suggested by Stevens et al. [6]. The other four peaks are identified as acoustic phonons of TA(X) at 0.68 THz, LA(X) at 1.02 THz, LA(Λ) at 1.42 THz, and LA(T) at 1.76 THz, respectively [16–18]. An optical phonon can emit two acoustic phonons as proposed by Menéndez and Cardona [19]. Here, it is possible that two LA(Λ) phonons with equal energy are emitted by a single A_{1g} phonon since the frequency of the LA(Λ) phonon is half of that of the A_{1g} phonon, and one LA(T) phonon and one LA(X) phonon are emitted by one A_{1g} phonon since the combined energy of LA(T) and LA(X) phonons equals to the energy of A_{1g}. The TA(X) phonon could be generated by a more complex process of three phonon coupling such as 2LA(X) − LA(Λ). Peaks in low frequency could also be affected by possible ripples introduced by Fourier Transform. Further investigations are needed to find the origin of these phonon modes.

In summary, the coherent phonon in Bi irradiated by ultrafast pulses is studied through time-resolved reflectivity measurements. It is found that the coherent phonon A_{1g} is generated by a combined process of ISRS and DECP. Acoustic phonons are also observed at high laser fluence, which is attributed to the energy relaxation of the A_{1g} phonon.

Acknowledgement

Support from the National Science Foundation is gratefully acknowledged.

References

[1] T.K. Cheng, S.D. Brorson, A.S. Kazeroonian, J.S. Moodera, G. Dresselhaus, M.S. Dresselhaus, E.P. Ippen, Appl. Phys. Lett. 57 (1990) 1004.
[2] T.K. Cheng, J. Vidal, H.J. Zeiger, G. Dresselhaus, M.S. Dresselhaus, E.P. Ippen, Appl. Phys. Lett. 59 (1991) 1923.
[3] H.J. Zeiger, J. Vidal, T.K. Cheng, E.P. Ippen, G. Dresselhaus, M.S. Dresselhaus, Phys. Rev. B 45 (1992) 768.
[4] K.S. Tinten, C. Blome, J. Blums, A. Cavalleri, C. Dietrich, A. Tarasevitch, I. Uschmann, E. Forster, M. Kammler, M. Horn-von-Hoegen, D. Linde, Nature 422 (2003) 287.
[5] G.A. Garrett, T.F. Albrecht, J.F. Whitaker, R. Merlin, Phys. Rev. Lett. 77 (1996) 3661.
[6] T.E. Stevens, J. Kuhl, R. Merlin, Phys. Rev. B. 65 (2002) 144304.

[7] A.Q. Wu, I.H. Chowdhury, X. Xu, Phys. Rev. B. 72 (2005) 085128.
[8] S. Hunsche, H. Kurz, Appl. Phys. A 65 (1997) 221.
[9] S. Hunsche, K. Wienecke, T. Dekorsy, H. Kurz, Phys. Rev. Lett. 75 (1995) 1815.
[10] M.F. DeCamp, D.A. Reis, P.H. Bucksbaum, R. Merlin, Phys. Rev. B 64 (2001) 092301.
[11] C.K. Sun, F. Vallée, L. Acioli, E.P. Ippen, J.G. Fujimoto, Phys. Rev. B. 48 (1993) 12365.
[12] O.V. Misochko, M. Hase, K. Ishioka, M. Kitajima, Phys. Rev. Lett. 92 (2004) 197401.
[13] S. Fahy, D.A. Reis, Phys. Rev. Lett. 93 (2004) 109701.
[14] C. Li, T. Sjodin, H. Dai, Phys. Rev. B 56 (1997) 15252.
[15] P. Tangney, S. Fahy, Phys. Rev. B 65 (2002) 054302.
[16] R.E. Macfarlane, in: D.L. Carter, R.T. Bate (Eds.), The Physics of Semimetal and Narrow Gap Semiconductors, Pergamon, New York, 1971, p. 289.
[17] J.L. Yarnell, J.L. Warren, R.G. Wenzel, S.H. Koenig, IBM J. Res. Dev. 8 (1964) 234.
[18] E.H. Poniatowski, M. Jouanne, J.F. Morhange, M. Kanehisa, R. Serna, C.N. Afonso, Phys. Rev. B 60 (1999) 10080.
[19] J. Menéndez, M. Cardona, Phys. Rev. B 29 (1984) 2051.